Society For Biomaterials

# Binding affinity of surface functionalized gold nanoparticles to hydroxyapatite

**Ryan D. Ross, Ryan K. Roeder**

Department of Aerospace and Mechanical Engineering, Bioengineering Graduate Program, University of Notre Dame, Notre Dame, Indiana 46556

Received 14 October 2010; revised 29 April 2011; accepted 11 May 2011
Published online 25 July 2011 in Wiley Online Library (wileyonlinelibrary.com). DOI: 10.1002/jbm.a.33165

**Abstract:** Gold nanoparticles (Au NPs) have been investigated for a number of biomedical applications, including drug and gene delivery vehicles, thermal ablation therapy, diagnostic sensors, and imaging contrast agents. Surface functionalization with molecular groups exhibiting calcium affinity can enable targeted delivery of Au NPs to calcified tissue, including damaged bone tissue. Therefore, the objective of this study was to investigate the binding affinity of functionalized Au NPs for targeted delivery to bone mineral, using hydroxyapatite (HA) crystals as a synthetic analog *in vitro*. Au NPs were synthesized to a mean particle size of 10–15 nm and surface functionalized with either L-glutamic acid, 2-aminoethylphosphonic acid, or alendronate, which exhibit a primary amine for binding gold opposite carboxylate, phosphonate, or bisphosphonate groups, respectively, for targeting calcium. Bisphosphonate functionalized Au NPs exhibited the most rapid binding kinetics and greatest binding affinity to HA, followed by glutamic acid and phosphonic acid. All functional groups reached complete binding after 24 h. Equilibrium binding constants in de-ionized water, determined by nonlinear regression of Langmuir isotherms, were 3.40, 0.69, and 0.25 mg/L for bisphosphonate, carboxylate, and phosphonate functionalized Au NPs, respectively. Functionalized Au NPs exhibited lower overall binding in fetal bovine serum compared to de-ionized water, but relative differences between functional groups were similar.  J Biomed Mater Res Part A: 99A: 58–66, 2011.

**Key Words:** gold nanoparticles, hydroxyapatite, binding affinity, targeted delivery, contrast agent, bisphosphonate

**How to cite this article**: Ross RD, Roeder RK. 2011. Binding affinity of surface functionalized gold nanoparticles to hydroxyapatite. J Biomed Mater Res Part A 2011:99A:58–66.

## INTRODUCTION

Gold nanoparticles (Au NPs) have been investigated for a number of biomedical applications,[1,2] including drug and gene delivery vehicles,[3,4] thermal ablation therapies,[4,5] diagnostic sensors,[6,7] and imaging contrast agents.[8–11] The utility of Au NPs in these applications is derived from multiple factors including the ease of synthesizing monodispersed nanoparticles, colloidal stability, biocompatibility, surface plasmon resonance, and high X-ray attenuation. Moreover, Au NPs are readily surface functionalized with molecular groups for cellular targeting and delivery, as well as enhancing colloidal stability. Surface functionalization with molecular groups exhibiting calcium affinity could enable targeted delivery of Au NPs to mineralized tissue, including fatigue microdamage in bone tissue,[12] as well as calcifications in soft tissue associated with cancer or musculoskeletal injury.

Microdamage accumulates in bone tissue during repetitive loading in the form of microcracks and diffuse damage.[13,14] The accumulation of microdamage has been implicated in clinical fracture susceptibility, including fatigue fractures in active individuals, such as military recruits, fragility fractures in the elderly, and the effects of long-term antiresorptive treatments for osteoporosis.[13,14] However, the role of microdamage in clinical bone fragility remains poorly understood due, in part, to limitations in available methods for detection and imaging.[14]

Current methods for imaging microdamage in bone tissue are limited to histological sections, which are inherently two-dimensional (2-D), destructive, invasive, and tedious.[15] The first and most common method has been *en bloc* staining with basic fuchsin in ethanol.[15–17] Basic fuchsin exhibits protein affinity, but primarily acts as a space-occupying dye.[15] Therefore, microdamage must be distinguished from nonspecific staining under observation in transmitted light or epifluorescent microscopy. More recently, fluorophores, such as xylenol and calcein, which employ iminodiacetate moieties for calcium-chelation, have been used as damage-specific labels for epifluorescent microscopy.[15,18,19] Moreover, sequential labeling with fluorophores exhibiting differing binding affinity enabled the measurement of spatiotemporal variation in damage events, including crack propagation[18,19] and modes of loading.[20] Additionally, calcium-specific photoinduced electron transfer sensor molecules have been

**Correspondence to:** R. K. Roeder; e-mail: rroeder@nd.edu
Contract grant sponsors: US Army Medical Research and Materiel Command (W81XWH-06-1-0196) though the Peer Reviewed Medical Research Program (PR054672)

 

investigated for the ability to "switch-on" fluorescence upon chelation to calcium ions in damaged tissue.[21,22] However, both light and epifluorescent microscopy are inherently 2-D. Three-dimensional (3-D) spatial information can only be ascertained from serial sectioning,[23,24] which is destructive and tedious. Laser scanning confocal microscopy has been used to provide limited depth of field for 3-D imaging of damage in histological sections labeled with fluorophores.[25,26]

X-ray computed tomography has been proposed for non-destructive and 3-D imaging of damage using contrast agents with higher X-ray attenuation than bone tissue. The presence, spatial variation, and accumulation of microdamage in both cortical and trabecular bone specimens was detected using micro-computed tomography (micro-CT) after staining tissue with a precipitated barium sulfate ($BaSO_4$) contrast agent.[27–29] While this technique enabled non-destructive and 3-D detection of microdamage *in vitro*, the precipitated $BaSO_4$ stain was not damage-specific and the staining solutions were not biocompatible. Iodinated molecules were investigated as a damaged-specific X-ray contrast agent,[30,31] but were only detected using micro-CT when precipitated in powder form.

Functionalized Au NPs were recently investigated as a targeted X-ray contrast agent for labeling microdamage in bone tissue.[12] Gold exhibits greater X-ray attenuation than other commonly used X-ray contrast agents containing barium and iodine.[32] Au NPs exhibited high X-ray attenuation and biocompatibility as an intravascular X-ray contrast agent in mice after intravenous administration.[9–11] Functionalized Au NPs also exhibit relatively high water solubility and low viscosity compared to iodinated molecular contrast agents. Finally, gold surfaces are readily functionalized through adsorption of thiols[33–35] and amines,[36–39] which can be used to attach molecules which target calcium ions on bone mineral crystals exposed on the surface of microcracks.

The objective of this study was to investigate the binding affinity of functionalized Au NPs for targeted delivery to bone mineral, using hydroxyapatite crystals as a synthetic analog *in vitro*. Au NPs were surface functionalized with either L-glutamic acid, 2-aminoethylphosphonic acid, or alendronate (Fig. 1). Glutamic acid is a naturally occurring amino acid with known affinity for calcium phosphates.[40,41] Moreover, glutamic acid functionalized Au NPs were previously shown to target damaged bone tissue.[12] However, phosphonate and particularly bisphosphonate groups are known to exhibit strong binding affinity to calcium phosphates.[42–44] Bisphosphonates, such as alendronate, are widely used clinically to suppress bone resorption as a pharmacological treatment for osteoporosis and other bone-related diseases.[14]

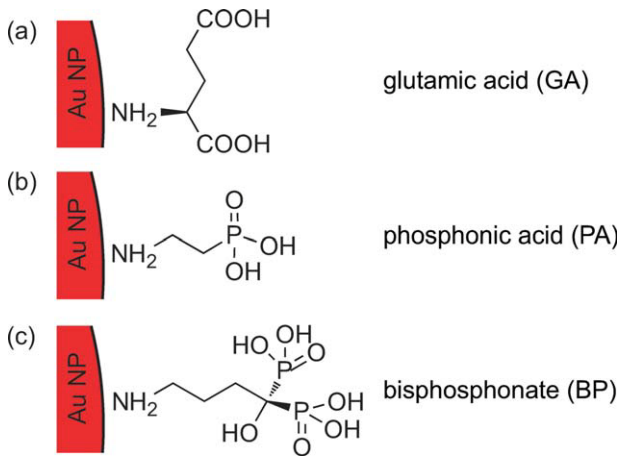


**FIGURE 1.** Gold nanoparticles (Au NPs) were surface functionalized with (a) L-glutamic acid, (b) 2-aminoethylphosphonic acid, or (c) alendronate, which exhibit a primary amine for binding to gold surfaces opposite (a) carboxylate, (b) phosphonate, or (c) bisphosphonate functional groups, respectively, for binding to calcium on bone mineral crystals exposed within damaged bone tissue. [Color figure can be viewed in the online issue, which is available at wileyonlinelibrary.com.]

## EXPERIMENTAL METHODS

### Gold nanoparticle synthesis and functionalization

Au NPs were synthesized to a mean particle diameter of 10–15 nm using the citrate reduction method.[45] Briefly, 0.1 g $HAuCl_4 \cdot 3H_2O$ ($\geq$99.9%, Aldrich) was added to 400 mL of de-ionized (DI) water and the solution was boiled vigorously while stirring. A 1% solution of trisodium citrate dehydrate (ACS reagent, >99.0%, Sigma) was added to the boiling solution at a mass ratio of 5:1 $HAuCl_4$ to sodium citrate and left boiling for an additional 20 min. The solution volume was then adjusted to a total of 500 mL using DI water. The resulting Au NP solution had a gold concentration of $\sim$0.5 m*M* and a wine red color.

Au NPs were prepared for functionalization by first removing excess citrate ions. 1.5 mL 2% polyvinyl alcohol (PVA 10–98, $M_W$ = 61,000, Fluka) was added to 24 mL Au NP solution, followed by 0.6 g ion exchange resin (Amberlite MB-150, Sigma). The resulting solution was stirred overnight and subsequently filtered (Grade 3, Whatman) to remove spent ion exchange resin. Au NPs were surface functionalized by adding 1 mL of a 0.01*M* solution of either L-glutamic acid ($\geq$99.5%, Fluka), 2-aminoethylphosphonic acid (99%, Aldrich), or alendronate sodium trihydrate ($\geq$97%, Sigma) (Fig. 1). The solution was left to equilibrate under mild stirring overnight. Excess functionalization molecules were removed by dialysis (Spectra/Por, MWCO = 3500, Spectrum Laboratories) against DI water for a total of 3 days, changing the water solution at least twice daily.

The mean particle diameter and particle size distributions were measured before and after functionalization by transmission electron microscopy (TEM, Hitachi H-600) at 75 kV accelerating voltage. TEM specimens were prepared by dropping a solution of functionalized Au NPs onto carbon-coated grids and evaporating the solvent. The particle diameter and aspect ratio were characterized by the mean and standard deviation from measurements on a total of 100 particles per functional group. Ultraviolet–visible (UV–vis) spectra (Varian Cary 3 spectrophotometer) were collected before and after functionalization to verify colloidal stability and relative concentrations of the particles within solution.

Surface functionalization of Au NPs was qualitatively verified using diffuse reflectance infrared Fourier transform

spectroscopy (DRIFTS, Bruker Tensor 27) at 4 $cm^{-1}$ with 64 total scans. Particles were functionalized and dialyzed as outlined above, except without the presence of PVA and without the use of ion exchange resin prior to functionalization and dialysis, in order to prevent PVA from interfering with the detection of functional groups. After dialysis, functionalized Au NPs were collected by evaporation at 40°C and 25 in Hg below atmospheric pressure. The dried powders were diluted in KBr (IR grade, 99+%, Acros Organics) at a ratio of ~1:200 by mass. Fourier transform infrared (FTIR) spectra were collected over frequencies of 4000–500 $cm^{-1}$ and normalized to the background spectra for KBr alone. FTIR peaks used to identify functional groups on Au NPs were determined by comparison to corresponding FTIR spectra for stock solutions of the functional molecules.

The amount of the three functional molecules (Fig. 1) adsorbed to Au NP surfaces was quantitatively measured using electrospray ionization mass spectrometry (ESI-MS). After the overnight functionalization step described above, 1 mL aliquots of the surface functionalized Au NP solution were removed and centrifuged at ~24,000*g* for 30 min to separate nanoparticles from the supernatant solution which included unbound functional molecules. The concentration of unbound functional molecules remaining in supernatant solutions was measured using ESI-MS (Bruker micro-TOF-QII) with calibration by serial dilution of functional molecule solutions. Glutamic acid and phosphonic acid samples were measured in positive ion mode, while bisphosphonate samples were measured in negative ion mode, with a capillary voltage of ±3.8–4.5 kV, a nebulizer gas pressure of 0.4 bar, a dry gas flow rate of 4.0 L/min, and a continuous sample flow rate of 4 μL/min. Spectra were collected over a range of 50–3000 $m/z$ at a rate of 5000 $s^{-1}$ for a period of 5 min. The amount adsorbed to Au NP surfaces was measured in triplicate and reported as the mean (± standard deviation) in μmol functional group per mg gold.

### Binding affinity of functionalized Au NPs

Two separate binding experiments were performed to investigate the binding affinity of functionalized Au NPs to bone mineral, using hydroxyapatite (HA) crystals as a synthetic analog. Calcium-deficient HA single crystal whiskers were synthesized using the chelate decomposition method, as described in detail elsewhere.[46] As-synthesized HA crystals exhibited a mean length of ~18 μm and mean width of ~2 μm.[46] The specific surface area of the crystals was 5.63 $m^2/g$ as measured by Brunauer–Emmett–Teller (BET) $N_2$ adsorption (Autosorb-1, Quantachrome Instruments).

The first set of experiments investigated the kinetics of binding. HA whiskers (10 ± 0.1 mg) were added to DI water, followed by a measured volume of functionalized Au NP solution, for a final volume of 15 mL containing a gold concentration of 0.1 mg/L. Solutions were placed onto a test tube rotator and allowed to incubate for 0.25, 0.5, 1, 2, 4, 8, 12, and 24 h. After the predetermined time, solutions were centrifuged at ~700*g* for 2 min to separate HA crystals and bound Au NPs from Au NPs remaining in solution. Percent binding was defined as the concentration (mg Au/L) of Au NPs remaining in the supernatant solution after binding, subtracted from the initial concentration of Au NPs in solution, and divided by the initial concentration of Au NPs. Binding of functionalized Au NPs to the surface of HA crystals was verified by TEM after dispersing the collected HA crystals onto carbon-coated grids.

A second set of experiments investigated the effect of concentration on binding affinity by plotting the binding isotherm for each functional group. The binding affinity of functionalized Au NPs to HA crystals was determined separately in DI water and 10% fetal bovine serum (FBS, Omega Scientific). The binding affinity of as-synthesized, citrate stabilized Au NPs was also measured as a control. Experiments were performed using the same methods outlined above for the binding kinetics, except the incubation time was held constant at 4 h and the initial gold concentration was varied. The kinetics of binding revealed that after 4 h 30–80% of Au NPs were bound to HA crystals depending on the functional group. This incubation time was also comparable to previous studies investigating bisphosphonate functionalized protein binding to HA surfaces.[43,44]

Binding isotherms were plotted as the amount of gold bound per mass of HA crystals added, $V$ (mg Au/g HA), versus the initial gold concentration, [S] (mg Au/L), for both DI water and FBS. Plotted binding data were modeled as a Langmuir isotherm,

$$V = \frac{V_{max}[S]}{K + [S]} \quad (1)$$

where $V$ is the amount of functionalized Au NPs bound per mass of HA crystals (mg/g), $V_{max}$ is the maximum surface binding (mg/g), [S] is the initial concentration of gold (mg/L), and $K$ is the equilibrium binding constant (mg/L). The equilibrium binding constant, $K$, and maximum binding of functionalized Au NPs on HA crystals, $V_{max}$, were measured from Langmuir isotherms using nonlinear least squares regression.

The gold concentration in control and supernatant solutions was measured using inductively coupled plasma-optical emission spectroscopy (ICP-OES, Optima 7000, PerkinElmer). Solutions were acidified to 2% v/v HCl prior to analysis. Calibration curves were created by diluting certified standard gold solutions (SPEX CertiPrep). All binding tests were performed at least in triplicate, reporting the mean and first standard deviation.

## RESULTS AND DISCUSSION

### Characterization of functionalized Au NPs

Functionalized Au NPs were spherical and relatively monodispersed (Fig. 2). There was no apparent change in particle size or morphology between as-synthesized and functionalized Au NPs. The mean (±standard deviation) particle diameter was 13.4 (1.2) nm for as-synthesized Au NPs, with an aspect ratio of 1.1 (0.1). The mean (±standard deviation) particle diameter was 11.4 (1.4), 13.6 (1.4), and 12.8 (1.6) nm for glutamic acid [Fig. 2(a)], phosphonic acid [Fig. 2(b)], and bisphosphonate [Fig. 2(c)] functionalized Au NPs,

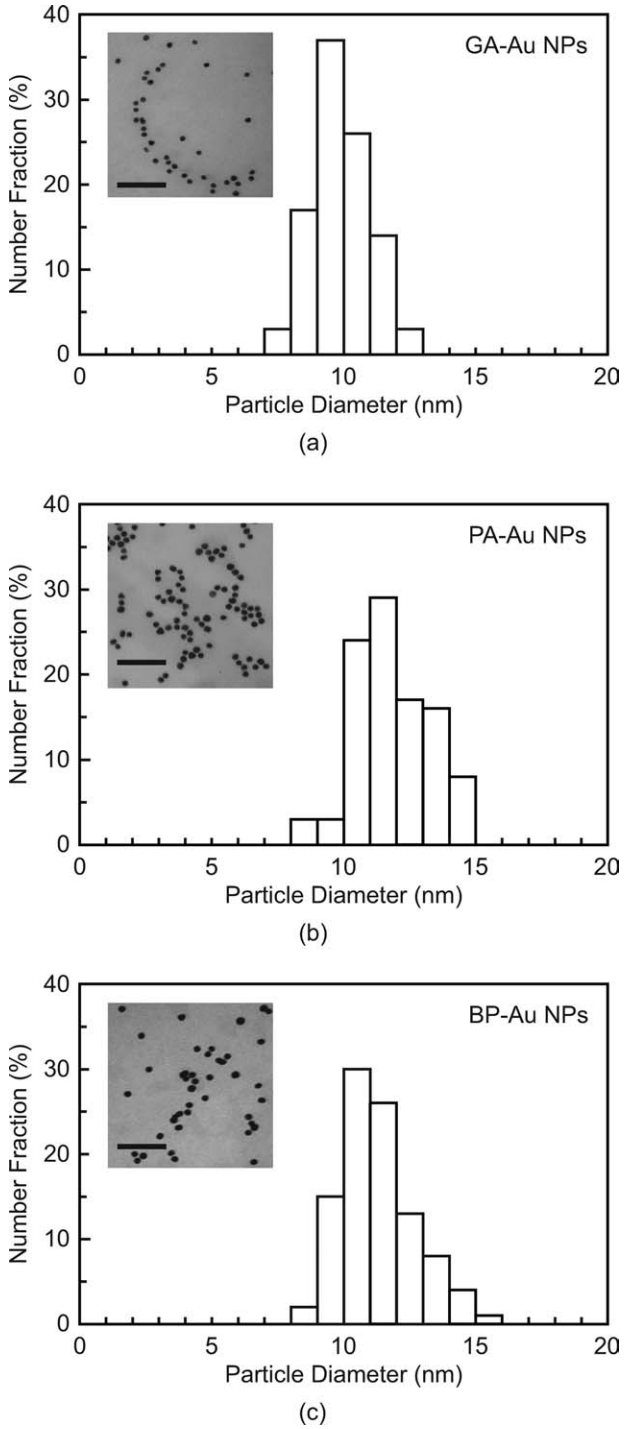


**FIGURE 2.** Particle size distributions and representative TEM micrographs of (a) glutamic acid (GA), (b) phosphonic acid (PA), and (c) bisphosphonate (BP) functionalized Au NPs. The scale bar in each micrograph represents 100 nm. The mean (±standard deviation) particle diameter was 11.40 (1.36), 13.57 (1.43), and 12.79 (1.58) nm for GA-, PA-, and BP-Au NPs, respectively.

respectively, with a mean (±standard deviation) aspect ratio of 1.1 (0.1) for each group. The plasmon resonance peak remained constant at ~530 nm for functionalized Au NPs, indicating that the colloidal suspension remained stable after functionalization (Fig. 3). The plasmon resonance band broadened slightly upon surface functionalization, due to the adsorption of amine groups.

Gold surface adsorption was expected to occur through the terminal amine group present in each functional molecule (Fig. 1). Previous studies have reported that the amine–gold surface interaction is facilitated by a weak covalent bond and an electrostatic complex between protonated amine groups and chloroaurate ions.[36–39] Adsorption of terminal amines facilitated the availability of carboxylate, phosphonate, and bisphosphonate groups for binding to calcium on HA crystals, which was qualitatively verified by FTIR (Fig. 4). Characteristic peaks for primary amines (3400–3500 $cm^{-1}$, N—H stretch; 1500–1650 $cm^{-1}$, N—H scissoring) were apparent for stock solutions of functional molecules, but were not apparent for functionalized Au NPs. A broad hydroxyl peak (2500–3600 $cm^{-1}$, O—H stretch) was present in all spectra. As-synthesized, citrate stabilized Au NPs and phosphonic acid functionalized Au NPs also exhibited peaks corresponding to alkyl groups (2850 and 2920 $cm^{-1}$, C—H stretch) which were not apparent for glutamic acid and bisphosphonate functionalized Au NPs. Carbonyl peaks (~1600 and 1710–1730 $cm^{-1}$, C=O stretch) were most prominent for glutamic acid functionalized and as-synthesized, citrate stabilized Au NPs. Phosphonic acid and bisphosphonate functionalized Au NPs exhibited peaks corresponding to phosphonyl groups (1220–1260 $cm^{-1}$, P=O stretch; 2500–2700 $cm^{-1}$, PO—H stretch). The location of these peaks were similar to a previous study on phosphonic acid functionalized Au NPs.[47] Taken together, the FTIR spectra suggested that Au NPs exhibited the intended terminal surface functionality, but did not quantify the amount of functional molecules adsorbed to Au NP surfaces.

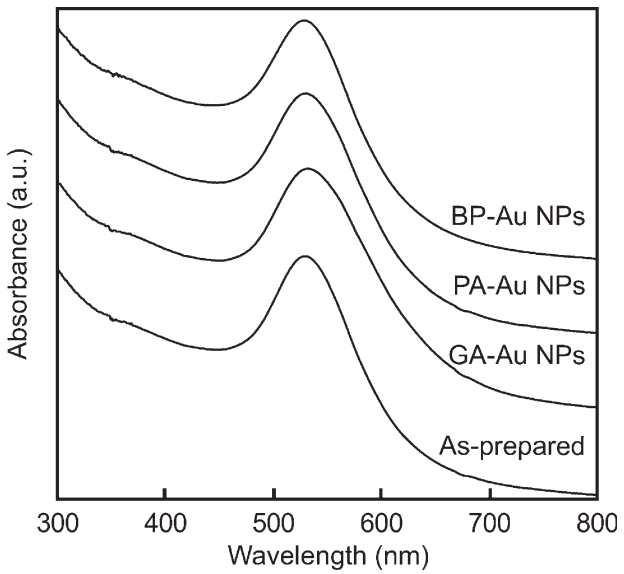


**FIGURE 3.** UV–vis spectra of as-synthesized Au NPs compared to glutamic acid (GA), phosphonic acid (PA), and bisphosphonate (BP) functionalized Au NPs, showing a consistent plasmon resonance peak at ~530 nm, which indicated that the particle size did not change and the colloid was stable after surface functionalization.

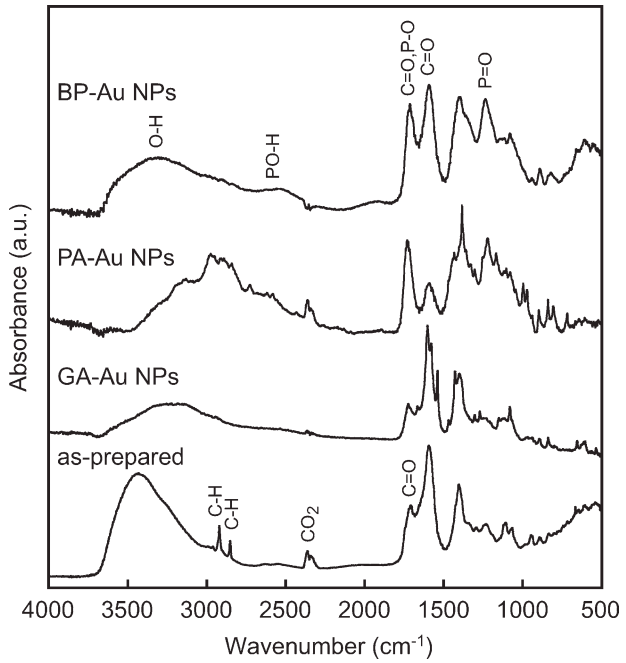


**FIGURE 4.** FTIR spectra of as-synthesized, citrate stabilized Au NPs compared to glutamic acid (GA), phosphonic acid (PA), and bisphosphonate (BP) functionalized Au NPs, confirming the presence of functional groups on gold surfaces. As-synthesized, citrate stabilized Au NPs and GA-Au NPs exhibited carboxylate functionality, while PA- and BP-Au NPs exhibited phosphonate functionality. Note that all peaks were verified by comparison to corresponding FTIR spectra for stock solutions of the functional molecules.

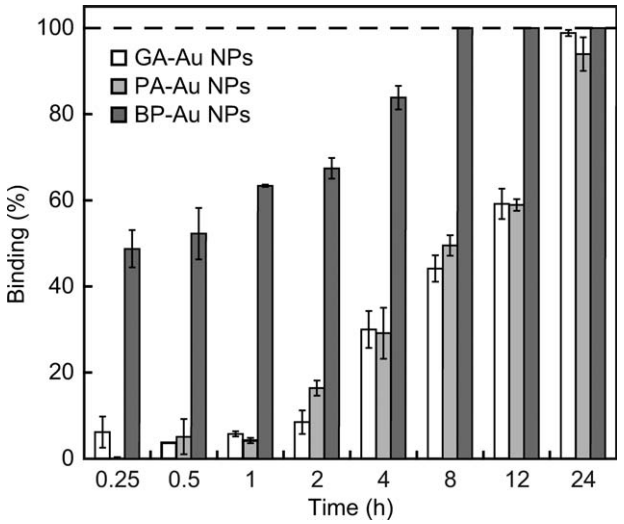


**FIGURE 6.** Binding kinetics of glutamic acid (GA), phosphonic acid (PA), and bisphosphonate (BP) functionalized Au NPs to HA crystals in DI water, showing the mean mass percent of Au NPs bound as a function of incubation time. Error bars show one standard deviation. Percent binding was defined as the concentration (mg Au/L) of Au NPs remaining in the supernatant solution after binding, subtracted from the initial concentration of Au NPs in solution, and divided by the initial concentration of Au NPs.

The mean (± standard deviation) amount of functional molecules adsorbed to glutamic acid, phosphonic acid, and bisphosphonate functionalized Au NP surfaces was 5.01 (0.02), 4.96 (0.02), and 3.25 (0.14) μmol/mg Au, respectively, as measured by ESI-MS. Therefore, the surface density of glutamic acid and phosphonic acid was similar and ~50% greater than bisphosphonate. The lower surface density of bisphosphonate molecules adsorbed to Au NP surfaces was likely due to steric interactions given the larger size of bisphosphonate molecules compared to glutamic acid and phosphonic acid (Fig. 1).

### Functionalized Au NP binding to HA crystals

Binding of functionalized Au NPs to HA crystal surfaces was confirmed by direct observation in TEM (Fig. 5). The number of Au NPs bound to HA crystal surfaces was comparatively greatest for bisphosphonate functionalized Au NPs followed by glutamic acid and phosphonic acid. Bisphosphonate functionalized Au NPs exhibited more rapid binding kinetics compared to glutamic acid or phosphonic acid functionalized Au NPs, reaching complete binding after 8 h in DI water (Fig. 6). Glutamic acid and phosphonic acid functionalized Au NPs exhibited similar binding kinetics, reaching near complete binding by 24 h in DI water. Thus, kinetic tests suggested differences in binding affinity between different functional groups, requiring further binding experiments.

Binding affinity isotherms for functionalized Au NPs exhibited large differences between functional groups

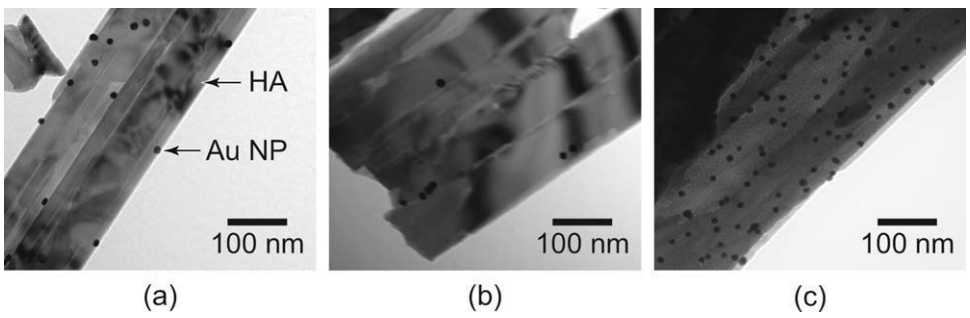


**FIGURE 5.** TEM micrographs showing (a) glutamic acid (GA), (b) phosphonic acid (PA), and (c) bisphosphonate (BP) functionalized Au NPs bound to the surface of HA crystals after 4 h in a solution containing a gold concentration of 0.1 mg/L in DI water.

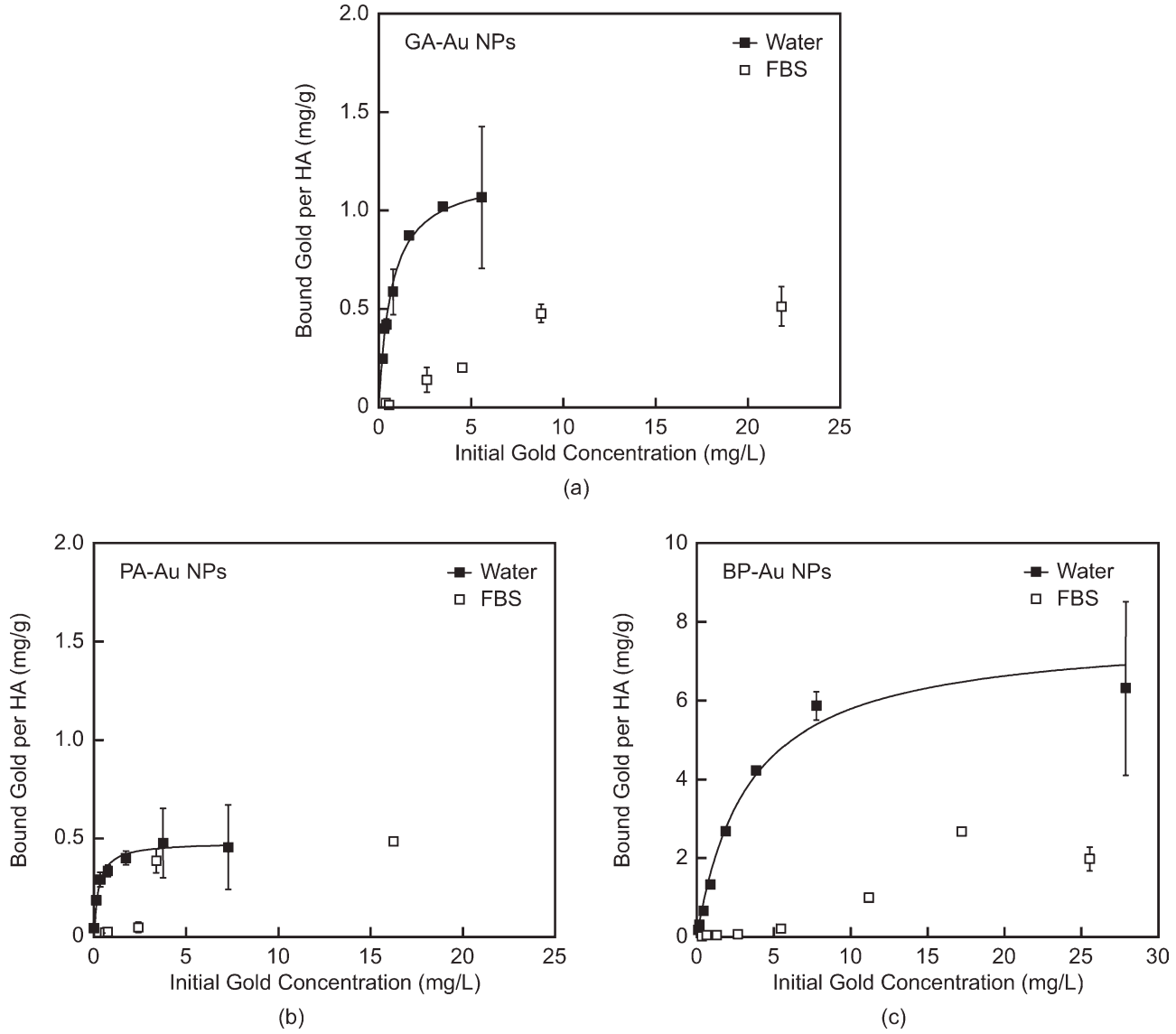


**FIGURE 7.** Binding isotherms for (a) glutamic acid (GA), (b) phosphonic acid (PA), and (c) bisphosphonate (BP) functionalized Au NPs in both DI water and FBS. Note that the scale of axes is changed in (c) due to the significantly greater binding affinity of BP-Au NPs. Experimental data for binding in DI water were fit by a Langmuir model using Eq. (1) with the binding constants in Table I. Binding in FBS did not exhibit equilibrium binding due to competition of soluble species present within serum solutions.

**TABLE I. The Equilibrium Binding Constant, *K* (mg/L), Maximum HA Surface Binding, $V_{max}$ (mg Au/g HA), and Maximum HA Surface Binding Normalized to the Specific Surface Area of HA Crystals, $V^*_{max}$ (mg Au/m$^2$ HA), for Glutamic Acid (GA), Phosphonic Acid (PA), and Bisphosphonate (BP) Functionalized Au NPs Compared to As-Synthesized (Citrate Stabilized) Au NPs**

| Group | *K* (mg/L) | $V_{max}$ (mg/g) | $V^*_{max}$ (mg/m$^2$) | $R^2$ |
|---|---|---|---|---|
| GA-Au NPs | 0.69 | 1.20 | 0.21 | 0.88 |
| PA-Au NPs | 0.25 | 0.48 | 0.09 | 0.69 |
| BP-Au NPs | 3.40 | 7.75 | 1.38 | 0.95 |
| Au NPs | 2.14 | 0.39 | 0.07 | 0.75 |

Constants were determined by nonlinear least squares regression of Langmuir isotherms.

(Fig. 7). Bisphosphonate functionalized Au NPs exhibited the greatest binding affinity to the surface of HA crystals, as evidenced by a comparatively greater amount of gold bound per HA (mg/g) and greater saturation concentration. Binding isotherms for glutamic acid [Fig. 7(a)], phosphonic acid [Fig. 7(b)], and bisphosphonate [Fig. 7(c)] functionalized Au NPs in DI water exhibited correlation coefficients ($R^2$) of 0.88, 0.69, and 0.95, respectively, using a Langmuir model (Table I). The equilibrium binding constant, *K*, and the maximum surface binding, $V_{max}$, were greatest for bisphosphonate functionalized Au NPs followed by glutamic acid and phosphonic acid (Table I). The maximum surface binding was also normalized by the specific surface area of the HA crystals to obtain a measure of the maximum binding of

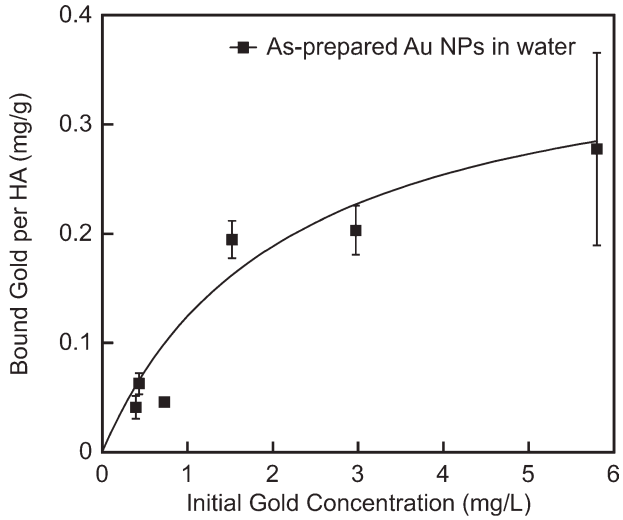


**FIGURE 8.** Binding isotherm for as-synthesized Au NPs in DI water. Experimental data was fit by a Langmuir model using Eq. (1) with the binding constants in Table I. The low binding affinity relative to functionalized Au NPs (Fig. 7) verified that binding was due to the calcium-specific functional groups rather than electrostatic interactions. Note that the scale of axes is different than Figure 7 due to a relatively low binding affinity.

functionalized Au NPs per surface area of HA, $V^*_{max}$ (mg Au/$m^2$ HA) (Table I).

As-synthesized Au NPs exhibited significantly lower binding affinity than the lowest of functionalized Au NPs in DI water (Table I) and therefore a relatively weak correlation to Langmuir kinetics ($R^2 = 0.75$) (Fig. 8). Therefore, differences in binding affinity between functional groups were attributed to the calcium-affinity of the functional group and not a simple electrostatic interaction.

The high binding affinity of bisphosphonate functionalized Au NPs was expected and consistent with previous studies investigating bisphosphonate functionalized model proteins, such as albumin,[42–44] and poly(D,L-lactide-*co*-glycolide) nanoparticles.[48] Other previous studies reported that molecules conjugated with eight aspartic acid or glutamic acid residues exhibited greater HA binding affinity compared to alendronate or pamidronate.[49,50] However, these results were likely due to a greater number of calcium binding sites per molecule compared to the single binding site present in a bisphosphonate molecule, and not necessarily due to the relative binding affinity of the functional groups themselves. In this study, alendronate functionalized Au NPs exhibited a six-fold greater binding affinity to HA compared to glutamic acid despite having ~50% fewer molecules adsorbed to Au NP surfaces (μmol/mg Au).

The overall binding affinity of functionalized Au NPs was decreased in FBS compared to DI water, but relative differences in binding affinity between functional groups remained consistent. However, the binding affinity of functionalized Au NPs in FBS was not able to be fit using any of the common adsorption models, including linear, Langmuir, Freundlich, or Brunauer, Emmett and Teller (BET) isotherms. Non-equilibrium binding behavior in serum solutions was also previously observed by Uludag et al.[42] Non-equilibrium binding of functionalized Au NPs to HA crystals in FBS may be attributed to a number of possible competitive binding effects, including (1) competition between soluble calcium ions and HA surfaces for binding functionalized Au NPs, (2) competition of soluble proteins and functionalized Au NPs for HA surfaces, (3) interactions between bound Au NPs through shared interactions with either soluble calcium or soluble proteins, (4) place-exchange reactions between functional groups and thiol or amine containing proteins in solution, or (5) some combination of these mechanisms. Note that serum proteins have been shown to rapidly coat Au NP surfaces, resulting in a change in the hydrodynamic diameter and zeta potential,[51] which could contribute to blocking functional group binding sites.

### Implications for targeted delivery

A damage-specific X-ray contrast agent could enable non-invasive and 3-D imaging of fatigue microdamage in bone. The results of this study suggest that, of the functional groups investigated, bisphosphonate functionalized Au NPs would provide the highest surface density (cf., Table I) of Au NPs labeling damaged bone tissue and, therefore, the greatest contrast enhancement in X-ray tomography. This will be verified in future work. Fatigue microcracks in human cortical bone specimens labeled by bisphosphonate functionalized Au NPs were able to be detected by synchrotron X-ray tomography in a preliminary study.[52] On the other hand, release and clearance of the contrast agent in clinical use might benefit from functional groups with intermediate binding affinity, similar to L-glutamic acid in this study. For example, γ-carboxyglutamic acid is a post-translationally modified amino acid which has been identified in proteins with hydroxyapatite affinity.[53] Further work will be required to determine the appropriate balance between the contrast enhancement and clearance of the agent. The significance of the present study was in demonstrating the ability to tailor and quantify the binding affinity for these objectives.

An additional concern for the use of bisphosphonate functionalized Au NPs as an imaging contrast agent is the pharmacological activity of bisphosphonates, which are commonly used to treat osteoporosis by inhibiting the cellular remodeling process to prevent additional loss of bone mass. The mechanism by which bisphosphonates are able to inhibit osteoclast activity is directly related to the presence of nitrogen.[54] Nitrogen-containing bisphosphonates, such as alendronate, have been shown to selectively inhibit a specific enzymatic pathway necessary for osteoclast function, while bisphosphonates that do not contain nitrogen are incorporated into toxic ATP analogs that cause apoptosis.[54] However, the nitrogen in alendronate is in the form of a primary amine, which was bound to the surface of Au NPs. Therefore, the pharmacological activity may have been passivated. The effects of amine binding to gold surfaces on cellular activity is unknown and will depend on potential intracellular place-exchange reactions between thiol and amine-containing molecules.[1,3]

Amongst the expansive body of research for active targeting of Au NPs for biological applications,[1–4] there has not, to our knowledge, been prior investigation on the binding affinity of functionalized Au NPs for mineralized tissue. While the main motivation for this study was in the use of Au NPs as a targeted contrast agent for labeling damaged bone tissue, other applications are readily envisioned for the detection of calcifications in soft tissue associated with cancer or musculoskeletal injury, and as drug delivery vehicles.

## CONCLUSIONS

Au NPs were synthesized to a mean particle diameter of 10–15 nm and surface functionalized with either L-glutamic acid, 2-aminoethylphosphonic acid, or alendronate, which exhibit a primary amine for gold surface adsorption opposite carboxylate, phosphonate, or bisphosphonate groups, respectively, for targeting calcium. Bisphosphonate functionalized Au NPs exhibited the most rapid binding kinetics and greatest binding affinity to HA, followed by glutamic acid and phosphonic acid. Functionalized Au NPs exhibited lower overall binding in FBS compared to de-ionized water, but relative differences between functional groups were similar. The high binding affinity of bisphosphonate functionalized Au NPs to HA could lead to improved labeling of damage bone tissue and enhanced-contrast in X-ray tomography.

## ACKNOWLEDGMENTS

This research was supported by the U.S. Army Medical Research and Materiel Command (W81XWH-06-1-0196) through the Peer Reviewed Medical Research Program (PR054672). The authors acknowledge the University of Notre Dame Center for Environmental Science and Technology (CEST) for the use of ICP-OES and UV–vis spectroscopy, the Mass Spectrometry and Proteomics Facility and William C. Boggess for the use of ESI-MS, and the Notre Dame Integrated Imaging Facility (NDIIF) for the use of TEM. Timothy L. Conrad is gratefully acknowledged for preparing the HA crystals used in binding experiments.

## REFERENCES

1. Sperling RA, Rivera Gil P, Zhang F, Zanella M, Parak WJ. Biological applications of gold nanoparticles. Chem Soc Rev 2008;37:1896–1908.
2. Huang X, Jain PK, El-Sayed IH, El-Sayed MA. Gold nanoparticles: Interesting optical properties and recent applications in cancer diagnostics and therapy. Nanomedicine 2007;2:681–693.
3. Ghosh P, Han G, De M, Kim CK, Rotello VM. Gold nanoparticles in delivery applications. Adv Drug Deliv Rev 2008;60:1307–1315.
4. Pissuwan D, Valenzuela SM, Cortie MB. Therapeutic possibilities of plasmonically heated gold nanoparticles. Trends Biotechnol 2006;24:62–67.
5. Hirsch LR, Stafford RJ, Bankson JA, Sershen SR, Rivera B, Price RE, Hazle JD, Halas NJ, West JL. Nanoshell-mediated near-infrared thermal therapy of tumors under magnetic resonance guidance. Proc Nat Acad Sci 2003;100:13540–13554.
6. Elghanian R, Storhoff JJ, Mucic RC, Letsinger RL, Mirkin CA. Selective colorimetric detection of polynucleotides based on the distance-dependent optical properties of gold nanoparticles. Science 1997;277:1078–1081.
7. Möller R, Fritzche W. Metal nanoparticle-based detection for DNA analysis. Curr Pharm Biotechnol 2007;8:274–285.
8. Hayat MA, editor. Colloidal Gold: Principles Methods and Applications, Vol. 1. San Diego: Academic Press; 1989.
9. Hainfeld JF, Slatkin DN, Focella TM, Smilowitz HM. Gold nanoparticles: A new X-ray contrast agent. Br J Radiol 2006;79:248–253.
10. Cai Q-Y, Kim SH, Choi KS, Kim SY, Byun SJ, Kim KW, Park SH, Juhng SK, Yoon KH. Colloidal gold nanoparticles as a blood-pool contrast agent for X-ray computed tomography in mice. Invest Radiol 2007;42:797–806.
11. Kim D, Park S, Lee JH, Jeong YY, Jon S. Antibiofouling polymer-coated gold nanoparticles as a contrast agent for *in vivo* X-ray computed tomography imaging. J Am Chem Soc 2007;129:7661–7665.
12. Zhang Z, Ross RD, Roeder RK. Preparation of functionalized gold nanoparticles as a targeted X-ray contrast agent for damaged bone tissue. Nanoscale 2010;2:582–586.
13. Burr DB, Forwood MR, Fyhrie DP, Martin RB, Schaffler MB, Turner CH. Bone microdamage and skeletal fragility in osteoporotic and stress fractures. J Bone Miner Res 1997;12:6–15.
14. Chapurlat BD, Delmas PD. Bone microdamage: A clinical perspective. Osteoporos Int 2009;20:1299–1308.
15. Lee TC, Mohsin S, Taylor D, Parkesh R, Gunnlaugsson T, O'Brien FJ, Giehl M, Gowin W. Detecting microdamage in bone. J Anat 2003;203:161–172.
16. Frost HM. Presence of microscopic cracks *in vivo* in bone. Henry Ford Hosp Med Bull 1960;8:25–35.
17. Burr DB, Hooser M. Alterations to the en bloc basic fuchsin staining protocol for the demonstration of microdamage produced *in vivo*. Bone 1995;17(4):431–433.
18. O'Brien FJ, Taylor D, Lee TC. An improved labelling technique for monitoring microcrack growth in compact bone. J Biomech 2002;35:523–526.
19. O'Brien FJ, Taylor D, Lee TC. Microcrack accumulation at different intervals during fatigue testing of compact bone. J Biomech 2003;36:973–980.
20. Wang X, Niebur GL. Microdamage propagation in trabecular bone due to changes in loading mode. J Biomech 2006;39:781–790.
21. Parkesh R, Mohsin S, Lee TC, Gunnlaugsson T. Histological, spectroscopic, and surface analysis of microdamage in bone: Toward real-time analysis using fluorescent sensors. Chem Mater 2007;19:1656–1663.
22. Parkesh R, Lee TC, Gunnlaugsson T. Fluorescence imaging of bone cracks (microdamage) using visibly emitting 1,8-naphthalimide-based PET sensors. Tetrahedron Lett 2009;50:4114–4116.
23. Mohsin S, O'Brien FJ, Lee TC. Microcracks in compact bone: A three-dimensional view. J Anat 2006;209:119–124.
24. Bigley RF, Singh M, Hernandez CJ, Kazakia GJ, Martin RB, Keaveny TM. Validity of serial milling-based imaging system for microdamage quantification. Bone 2008;42:212–216.
25. Zioupos P, Currey JD. The extent of microcracking and the morphology of microcracks in damaged bone. J Mater Sci 1994;29:978–986.
26. O'Brien FJ, Taylor D, Dickson GR, Lee TC. Visualization of three-dimensional microcracks in compact bone. J Anat 2000;197:413–420.
27. Wang X, Masse DB, Leng H, Hess KP, Ross RD, Roeder RK, Niebur GL. Detection of trabecular bone microdamage by micro-computed tomography. J Biomech 2007;40:3397–3403.
28. Leng H, Wang X, Ross RD, Niebur GL, Roeder RK. Micro-computed tomography of fatigue microdamage in cortical bone using a barium sulfate contrast agent. J Mech Behav Biomed Mater 2008;1:68–75.
29. Landrigan MD, Li J, Turnbull TL, Burr DB, Niebur GL, Roeder RK. Contrast-enhanced micro-computed tomography of fatigue microdamage accumulation in human cortical bone. Bone 2011;48:443–450.
30. Parkesh R, Gowin W, Lee TC, Gunnlaugsson T. Synthesis and evaluation of potential CT (computer tomography) contrast agents for bone structure and microdamage analysis. Org Biomol Chem 2006;4:3611–3617.
31. Parkesh R, Lee TC, Gunnlaugsson T, Gowin W. Microdamage in bone: Surface analysis and radiological detection. J Biomech 2006;39:1552–1556.
32. Hubbell JH, Seltzer SM. Table of X-ray Mass Attenuation Coefficients and Mass Energy-Absorption Coefficients (version 1.4). Gaithersburg, MD: National Institute of Standards and Technology; 2004. Available at http://physics.nist.gov/xaamdi.
33. Giersig M, Mulvaney P. Preparation of ordered colloid monolayers by electrophoretic deposition. Langmuir 1993;9:3408–3413.

34. Brust M, Walker M, Bethell D, Schiffrin DJ, Whyman R. Synthesis of thiol-derivated gold nanoparticles in a 2-phase liquid-liquid system. J Chem Soc Chem Commun 1994;7:801–802.
35. Brust M, Fink J, Bethell D, Schiffrin DJ, Kiely C. Synthesis and reactions of functionalised gold nanoparticles. J Chem Soc Chem Commun 1995: 1655–1656.
36. Leff DV, Brandt L, Heath JR. Synthesis and characterization of hydrophobic, organically-soluble gold nanocrystals functionalized with primary amines. Langmuir 1996;12:4723–2730.
37. Kumar A, Mandal S, Selvakannan PR, Pasricha R, Mandale AB, Sastry M. Investigation into the interaction between surface-bound alkylamines and gold nanoparticles. Langmuir 2003;19: 6277–6282.
38. Selvakannan PR, Mandal S, Phadtare S, Pasricha R, Sastry M. Capping of gold Nanoparticles by the amino acid lysine renders them water-dispersable. Langmuir 2003;19:3545–3549.
39. Aslam M, Fu L, Su M, Vijayamohanan K, Dravid VP. Novel one-step synthesis of amine-stabilized aqueous colloidal gold nanoparticles. J Mater Chem 2004:1795–1997.
40. Bolander ME, Young MF, Fisher LW, Yamada Y, Termine JD. Osteonectin cDNA sequence reveals potential binding regions for calcium and hydroxyapatite and shows homologies with both a basement membrane protein (SPARC) and a serine proteinase inhibitor (ovomucoid). Proc Natl Acad Sci 1988;85: 2919–2923.
41. Fujisawa R, Wada Y, Nodasaka Y, Kuboki Y. Acidic amino acid-rich sequences as binding sites of osteonectin to hydroxyapatite crystals. Biochim Biophys Acta 1996;1292:53–60.
42. Uludag H, Kousinioris N, Gao T, Kantoci D. Bisphosphonate conjugation to proteins as a means to impart bone affinity. Biotechnol Prog 2000;16:258–267.
43. Bansal G, Wright JEI, Zhang S, Zernicke RF, Uludag H. Imparting mineral affinity to proteins with thiol-labile disulfide linkages. J Biomed Mater Res A 2005;74:618–628.
44. Wright JEI, Gittens SA, Bansal G, Kitov PI, Sindrey D, Kucharski C, Uludag H. A comparison of mineral affinity of bisphosphonate-protein conjugates constructed with disulfide and thioether linkages. Biomaterials 2006;26:769–784.
45. Turkevich J, Stevenson PC, Hillier J. A study of the nucleation and growth processes in the synthesis of colloidal gold. Discuss Faraday Soc 1951;11:55–75.
46. Roeder RK, Converse GL, Leng H, Yue W. Kinetic effects on hydroxyapatite whiskers synthesized by the chelate decomposition method. J Am Ceram Soc 2006;89:2096–2104.
47. Fiurasek P, Reven L. Phosphonic and sulfonic acid-functionalized gold nanoparticles: A solid-state NMR study. Langmuir 2007;23: 2857–2866.
48. Choi SW, Kim JH. Design of surface-modified poly(D,L-lactide-*co*-glycolide) nanoparticles for targeted drug delivery to bone. J Control Release 2007;122:24–30.
49. Wang D, Miller S, Sima M, Kopecková P, Kopecek J. Synthesis and evaluation of water-soluble polymeric bone-targeting drug delivery systems. Bioconjug Chem 2003;14:853–859.
50. Murphy MB, Hartgerink JD, Goepferich A, Mikos AG. Synthesis and *in vitro* hydroxyapatite binding of peptides conjugated to calcium-binding moieties. Biomacromolecules 2007;8:2237–2243.
51. Alkilany AM, Nagaria PK, Hexel CR, Shaw TJ, Murphy CJ, Wyatt MD. Cellular uptake and cytotoxicity of gold nanorods: Molecular origin of cytotoxicity and surface effects. Small 2009;5:701–708.
52. Ross RD, Roeder RK. Functionalized gold nanoparticles for targeted labeling of damaged bone tissue in X-ray tomography. Trans Orthop Res Soc 2010;35:1368.
53. Price PA, Otsuka AS, Poser JW, Kristaponis J, Raman N. Characterization of a gamma-carboxyglutamic acid-containing protein from bone. Proc Natl Acad Sci USA 1976;73:1447–1451.
54. Reszka AA, Roda GA. Bisphosphonate mechanism of action. Curr Rheumatol Rep 2003;5:65–74.